

## MAGNITUDE OF REGGE CUT CONTRIBUTIONS IN THE TRIPLE-REGGE REGION

J. BARTELS and G. KRAMER

*II. Institut für Theoretische Physik der Universität Hamburg*

Received 22 September 1976

Starting from the reggeon calculus, the various possibilities of absorptive pomeron cut corrections in the triple-Regge region are considered. For the case of  $pp \rightarrow pX$ , we estimate their importance at present day energies. We conclude that at highest ISR energies, pomeron cuts of the eikonal type are not enough, and enhanced diagrams with at least one additional triple-pomeron coupling need be included.

### 1. Introduction

Recently several authors [1–6] have pointed out that a pure Regge-pole description of inclusive processes  $a + b \rightarrow c + \text{anything}$  in the triple-Regge region cannot account for the observed cross sections. In inclusive photo and electroproduction [1–4]  $\gamma + p \rightarrow \pi^{\pm,0} + X$ , the pure Regge-pole model predicts a zero in  $d^2\sigma/dp_{\perp}^2 dM^2$  at  $p_{\perp}^2 = 0$ . But such a dip has not been seen in the data. In the same reaction, recent measurements show a target asymmetry which a Regge-pole description without cuts cannot account for [3]. In describing the charge exchange reaction  $p(n) + p \rightarrow n(p) + X$  [5] by the exchange of Regge poles, all parameters of such a model are fixed from other reactions. Hence this process provides a good test for the Regge mechanism. However, the theoretical cross sections are too large in comparison with the data. All these failures of the Regge-pole model have been suggested to be cured by absorptive or cut corrections.

An even stronger need for cut corrections exists in pomeron dominated reactions such as  $pp \rightarrow pX$ . In a recent calculation [6], absorptive corrections to the pomeron pole exchange turned out to be considerably larger than one might expect from the experience with two-body reactions. For very large energies where reggeon field theory becomes applicable one knows [7] that even infinitely many pomeron cut contributions are necessary in order to yield a theory for hadron-hadron scattering that is free from inconsistencies. At present energies we are still outside of this asymptotic domain. But certainly some of these cut contributions which will be dominant for larger energies are relevant already at ISR energies. What these contri-

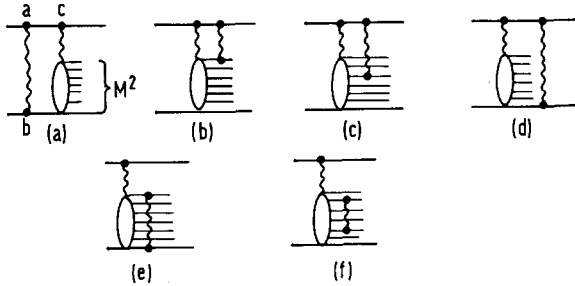


Fig. 1. Different types of initial and final state absorptive corrections.

butions are and how important they are at NAL or ISR energies needs still to be examined.

When computing corrections to the pure Regge-pole exchanges, most of the authors [1–5] have been guided by the idea of initial or final state absorption. Initial state absorption then easily leads to the pomeron exchange between the incoming particles a and b (fig. 1a). In the final state, however, there are several ways to include absorption: a pomeron can be exchanged between particle c and any of the cluster particles (figs. 1b, c, d) and, in addition to that between particles within the cluster (figs. 1e, f). The first contribution is fairly easily computed by means of the absorption formalism known from two-body reactions. Among the other pomeron corrections only that of fig. 1d has been included in existing papers. In ref. [2] the size of these absorption corrections has been treated as a free parameter, and it turned out to be much larger than predicted from fits to two-body reactions. This could indicate that in fact some of the other absorptive corrections need to be included in order to restore the consistency between two-body scattering and inclusive reactions. The main reason why these contributions have been disregarded so far, is that, within the *s*-channel language of initial or final state absorption, their computation is rather elaborate. A much more convenient way for their calculation is given by the reggeon calculus which recently [8,9] has been derived for the triple-Regge region. In order to make contact between this reggeon diagram technique and the picture of initial or final state absorption, one uses the cutting rules of Gribov et al. [10]. One then finds that, in addition to the absorptive corrections considered above, there are other contributions of the same size which need to be taken into account. It is the aim of this paper to make use of this reggeon calculus and discuss the various cut contributions to the triple-Regge region. In particular we want to get an idea of what kind of corrections are relevant at present day energies. To start with, we consider pomeron dominated processes and estimate the size of several reggeon graphs. Their relative importance is energy dependent, and at low energies ( $s \sim 100 \text{ GeV}^2$ ) one needs other cut contributions than at ISR energies ( $s = 3000 \text{ GeV}^2$ ). In particular we find that the eikonal formula which has been derived by several authors [4,6,11] is not an adequate description at highest ISR

energies. To make this paper as self-contained as possible, we first (sect. 2) list the rules of the reggeon calculus and demonstrate the connection with the picture of initial or final state absorption. Sect. 3 contains our estimates, whereas some details of our calculations are put into an appendix. In the final section we draw our conclusions. In a future paper, we will perform a similar analysis for some Regge-pole dominated reactions.

**2. Reggeon calculus and the absorption picture**

We start by listing the main rules of the reggeon calculus for the triple-Regge region. This reggeon diagram technique has recently been derived both from a partial-wave analysis [8] and from the high-energy behaviour of hybrid Feynman diagrams [9]. The starting point is Mueller's argument which relates the double differential inclusive cross section to the  $M^2$  discontinuity of a  $3 \rightarrow 3$  scattering amplitude (fig. 2)

$$\frac{d^2\sigma}{dt dM^2} = \frac{1}{32i\pi s^2} \text{disc}_{M^2} T_{3 \rightarrow 3}(s + i\epsilon, s - i\epsilon, M^2, t) . \tag{1}$$

For the  $3 \rightarrow 3$  amplitude we use a Sommerfeld-Watson representation:

$$\begin{aligned} T_{3 \rightarrow 3}(s + i\epsilon, s + i\epsilon, M^2 + i\epsilon, t) \\ = \frac{-1}{(2\pi i)^3} \int \int \int dj_1 dj_2 dj \xi_{j_1} s^{j_1} \xi_{j_2} s^{j_2} \xi_{jj_1j_2} (M^2)^{j-j_1-j_2} F(j_1, j_2, j, t) , \end{aligned} \tag{2}$$

where

$$\begin{aligned} \xi_{j_1} &= (e^{-i\pi j_1} + \tau_1) / \sin \pi j_1 , \\ \xi_{jj_1j_2} &= (e^{-i\pi(j-j_1-j_2)} + \tau_1\tau_2) / \sin \pi(j - j_1 - j_2) . \end{aligned} \tag{3}$$

In eq. (2) the three  $j$ -variables are the angular momenta of the three cross channels (fig. 3). Dual to each cross channel, one has a large energy variable and, associated with it, a signature factor.  $F(j_1, j_2, j, t)$  is the partial-wave amplitude and contains the singularities of Regge poles and cuts. In order to combine eqs. (1) and (2), we ob-

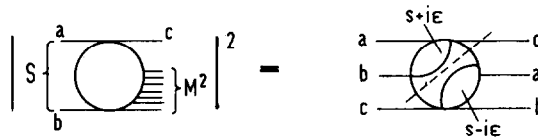


Fig. 2. Optical theorem for the inclusive cross section  $a + b \rightarrow c + \text{anything}$ .

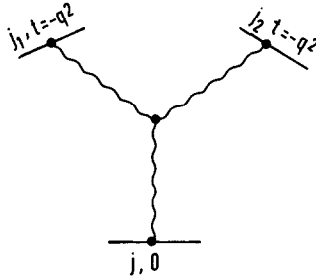


Fig. 3. Triple-Regge pole diagram.

serve the  $i\epsilon$  prescription in (1) and take the discontinuity in  $M^2$ . This leads us to

$$\frac{d^2\sigma}{dt dM^2} = \frac{1}{16\pi s^2} \frac{1}{(2\pi i)^3} \int_{c-i\infty}^{c+i\infty} \int \int dj_1 dj_2 dj \xi_{j_1} s^{j_1} \xi_{j_2}^* s^{j_2} \times (M^2)^{j-j_1-j_2} F(j_1, j_2, j, t). \tag{4}$$

The reggeon calculus for the triple-Regge region now states that any pole or cut contribution can be written in the form of eq. (4). Furthermore, it gives the rules how to compute the partial wave  $F$  for any given reggeon diagram. These rules are \*

(i) Replace the momentum transfer  $t$  by a two-dimensional spacelike momentum variable  $q$ ,  $q^2 = -t$ .

(ii) Like in an ordinary Feynman diagram, there is a  $k$ -integration  $\int d^2k/(2\pi)^2$  for each internal loop, and momentum is conserved at each vertex. The net momentum at the bottom of the diagram (fig. 3) is zero. At the two upper ends, the net momentum is  $q$ .

(iii) Any given reggeon diagram should be drawn in such a way that all reggeon lines point upwards. All reggeon vertices must be ordered from the bottom to the top of the diagram. In the example of fig. 4a, there is no ambiguity in ordering the reggeon vertices. In fig. 4b, the triple vertices 1 and 2 may occur in two configurations. Vertex 1 can be above vertex 2 (as shown in fig. 4b) or, alternatively, below vertex 2 (fig. 4c). Both configurations must be taken into account. One then finds in each diagram a uniquely defined “branching” vertex with the following property: it is the highest vertex in the diagram which connects the two branches leading to the upper right- and left-hand ends. In fig. 4a, the branching vertex is the central triple-Regge vertex. In figs. 4b and c it is vertex 1 and 2 respectively.

(iv) Passing through the diagram from the bottom to the top (fig. 4), draw a horizontal cutting line for each intermediate reggeon state. For a  $n$ -reggeon state

\* We use the formulation given in ref. [8].

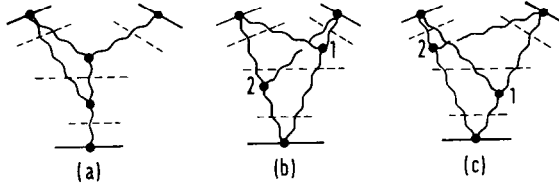


Fig. 4. Reggeon calculus for the triple-Regge region: the horizontal dotted lines denote the various intermediate states for which a factor  $[j + (n - 1) - \sum_{i=1}^n \alpha(k_i)]^{-1}$  is needed. (cf. the rules given in sect. 2).

below the branching vertex write a factor

$$[j + (n - 1) - \sum_{i=1}^n \alpha(k_i)]^{-1}. \quad (5)$$

For intermediate states of the upper left and right branch with  $n_1$  and  $n_2$  cut reggeon lines write

$$[j_1 + (n_1 - 1) - \sum_{i=1}^{n_1} \alpha(k_i)]^{-1}, \quad (6)$$

$$[j_2 + (n_2 - 1) - \sum_{i=1}^{n_2} \alpha(k_i)]^{-1}, \quad (7)$$

respectively. In eqs. (5)–(7)  $\alpha(k_i)$  are the trajectory functions of the reggeon lines intersecting with the horizontal cutting lines.

(v) For each 2-particle- $n$ -reggeon vertex write a factor  $(i)^{n-1} N_n$ . The branching vertex obtains the (real) factor  $r_b$ , and each of the remaining triple-Regge vertices is denoted by  $i r / \sqrt{2}$  (the  $\sqrt{2}$  is due to our definition of  $r$  in the pole diagram eq.(8)).

(vi) For the exchange of  $n$  indistinguishable reggeons put a factor  $1/n!$ .

We want to make a few comments about these rules. We have been using the word reggeon in order to indicate that these rules are valid not only for pomeron exchanges but also for reggeons such as  $\rho$ ,  $\pi$ , etc. The vertex factors  $N_n$  and  $r$  are, in general, functions of the momenta of the adjacent reggeon lines. What is important is that, except for the branching vertex they all are the same as in  $2 \rightarrow 2$  reactions. This leaves rather little freedom for the parameters of cut corrections in the triple-Regge limit.

After this brief review of the reggeon calculus we want to demonstrate in what sense initial and final state absorptive corrections are contained in reggeon diagrams. We apply the cutting rules of Gribov et al. [10] to the  $M^2$  discontinuity of the  $3 \rightarrow 3$  scattering amplitude and evaluate the discontinuity in one of the  $s$ -variables, say the left one. This is equivalent to considering the process  $a + b \rightarrow c + X$  as a two-body reaction and looking for the various  $s$ -channel discontinuities. As an example we analyse the graph of fig. 5a. Applying the argument of ref. [10] to the left-hand side of the diagram, we consider all possible ways of cutting the left-hand side from the

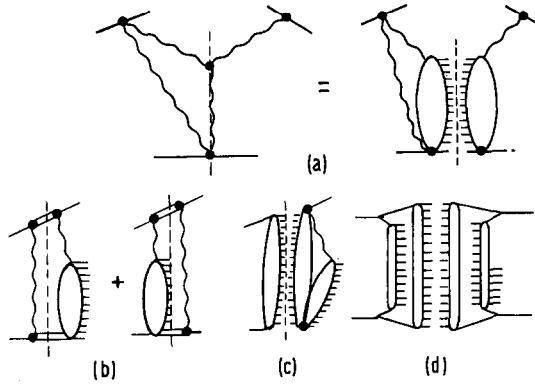


Fig. 5.  $M^2$  and  $s$ -discontinuities in a Regge-cut diagram. In (a) the cut denotes the  $M^2$  discontinuity according to eq. (1). In (b)–(d) we consider the part on the left-hand side of the cut (a) and take the discontinuity in  $s$ . (b) represents the diffractive cut, (c) the multiperipheral and (d) the double multiperipheral cut.

top vertex down to the bottom vertex. For the cutting line running between the reggeon lines, we obtain the intermediate states of fig. 5b. When the cut runs along one of the reggeon lines, we arrive at the configuration of fig. 5c. Finally, the cutting line may pass simultaneously along both reggeon lines, and this corresponds to fig. 5d. In fig. 5b we easily recognize the initial state absorption and one of these final state absorptions which we have described above (fig. 1a). The other types of final state absorption are obtained if we perform a similar cutting analysis for other reggeon graphs. From the analysis of fig. 5, however, we learn that other configurations than final or initial state absorption are of the same size and cannot be disregarded. The reggeon calculus automatically includes all these contributions.

### 3. Quantitative analysis of pomeron cuts in $pp \rightarrow pX$

In this section we use the reggeon calculus which we have described in sect. 2 in order to calculate various pomeron graphs for the process  $pp \rightarrow pX$ . In particular we are interested in the question which graphs are relevant at present day energies. This is not meant to be a fit to experimental data, but an attempt to classify the different types of pomeron cut corrections and estimate their size at available energies. Details of our calculations are contained in the appendix.

We start with the pole graph (fig. 3). Its contribution to  $d^2\sigma/dtdM^2$  is

$$\frac{1}{16\pi s^2} g^3(t) r(t) \left(\frac{s}{M^2}\right)^{2\alpha(t)} M^2 \left| \frac{e^{-i\pi\alpha(t)} + 1}{\sin \pi\alpha(t)} \right|^2. \quad (8)$$

We take  $\alpha(t) = 1 + \alpha't$  with  $\alpha' = 0.25 \text{ GeV}^{-2}$ . Calculations in reggeon field theory [12] have shown that in order to give the pomeron a renormalized intercept at one

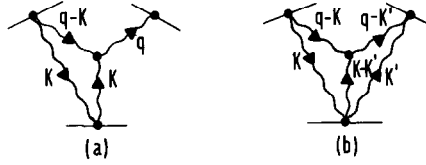


Fig. 6. Eikonal type pomeron cut corrections to the pole graph (eqs. (12) and (13)).

a bare intercept above one is needed. Using the value of ref. [12] for the shift of the intercept we found that up to ISR energies our results do not alter significantly if we use the critical intercept rather than 1. For the sake of simplicity we therefore will take the pomeron intercept at 1. For both the pomeron-particle-particle coupling  $g(t)$  and the tripe-pomeron coupling  $r(t_1, t_2, t_3)$  we assume an exponential  $t$ -dependence:

$$g(t) = g_0 e^{-A|t|/2}, \quad (9)$$

$$r(t_1, t_2, t_3) = r_0 e^{-B(|t_1|+|t_2|+|t_3|)/2}. \quad (10)$$

The values for the constants  $A$  and  $B$  are taken from ref. [6]:  $A = 3.5 \text{ GeV}^{-2}$ ,  $B = 1.0 \text{ GeV}^{-2}$ . For  $g_0$  and  $r_0$  we use  $g_0 = 10 \text{ GeV}^{-1}$ ,  $r_0 = 0.50 \text{ GeV}^{-1}$ . The value of  $r_0$  is taken from a pomeron pole fit to the inclusive cross-section data. This value, however, is uncertain by a factor of 2. Furthermore, our analysis will show that a pomeron pole fit to the data is not well justified, since pomeron cut contributions in the triple-Regge region are also very important. All this makes the numerical value for  $r$  rather uncertain. For our qualitative estimate we choose a value that lies roughly half-way between the lowest and highest value obtained from the pole fit. Using the expressions (9) and (10), we rewrite (8):

$$F_{\text{pole}} = \frac{g_0^3 r_0}{16\pi M^2 (\cos \frac{1}{2} \pi q^2)^2} \exp[-(A + B + 2\alpha' \ln(s/M^2))q^2]. \quad (11)$$

In the following we will, for simplicity, neglect the  $q^2$  dependence of the denominator and replace  $\cos \frac{1}{2} \pi q^2$  by 1.

Next we consider the graphs of fig. 6. The explicit calculations are given in the appendix. Here we only quote the results at  $q^2 = 0$ . For fig. 6a we obtain

$$F_{\text{pole}} \frac{g_0^2}{16\pi\alpha' [\ln s - \frac{1}{2}i\pi + (2A+B)/2\alpha']}, \quad (12)$$

and for the graph of fig. 6b

$$F_{\text{pole}} \left( \frac{g_0^2}{8\pi\alpha'} \right)^2 \times \frac{1}{4(\ln s - \frac{1}{2}i\pi + (2A+B)/2\alpha')(\ln s + \frac{1}{2}i\pi + (2A+B)/2\alpha') - (\ln M^2 + (A+B)/2\alpha')^2}. \quad (13)$$

$F_{\text{pole}}$  stands for the expression in eq. (11) at  $q^2 = 0$ , and we have presented our results in a form which emphasizes the size of pomeron cut diagrams relative to the pole contribution. In writing down the expressions for fig. 6a and fig. 6b, we encounter two-pomeron-two-particle and three-pomeron-two-particle coupling functions. They contain the finite-mass part of intermediate states of the pomeron-particle system. In a first approximation, one takes into account only the elastic intermediate state:

$$N_2(q^2, k^2, (q - k)^2) = g(k^2) g((q - k)^2) / \sqrt{2}, \tag{14}$$

$$N_3(q^2, k_1^2, k_2^2, (q - k_1 - k_2)^2) = \frac{1}{2} g(k_1^2) g(k_2^2) g((q - k_1 - k_2)^2). \tag{15}$$

A way to include inelastic contributions is to multiply (14) by a number  $\lambda > 1$  and (15) by  $\lambda^2$ . However, due to the relative smallness of inelastic contributions, this number  $\lambda$  is only slightly above one and does not affect the outcome of our analysis. We will therefore use (14) and (15). Another point we want to comment on is the signature and phase structure of our diagrams. In the representation (4), the entire phase structure is exhibited in the two signature factors, and the partial wave  $F$  is real. When the signature factors are written as

$$\xi_j = e^{-i\pi j/2} / \sin(\frac{1}{2}\pi j), \tag{16}$$

the whole phase structure is contained in the first factor on the right-hand side of eq. (16). Its influence on the size of our diagrams turns out to be very small. The results given in eqs. (12) and (13) have been calculated including the phase factors of eq. (16), and the result of this are the  $\frac{1}{2}i\pi$  terms in the denominators of (12) and (13). For the numerical estimate we neglect them.

Using the values for  $g_0, r_0, \alpha', A$  and  $B$  given above, we compute the factors multiplying  $F_{\text{pole}}$  in (12) and (13). They give the weight of the pomeron cuts relative

Table 1

Diagram	$s = 20$		$s = 1000$		$s = 3000$	
	$M^2 = 4$	$M^2 = 10$	$M^2 = 200$	$M^2 = 500$	$M^2 = 600$	$M^2 = 1500$
fig. 6a	-0.42	-0.42	-0.35	-0.35	-0.34	-0.34
fig. 6b	0.19	0.19	0.13	0.13	0.12	0.12
fig. 3+2 × fig. 6a + fig. 6b	0.35	0.35	0.43	0.43	0.44	0.44
fig. 8a	-0.04	-0.07	-0.14	-0.17	-0.16	-0.19
fig. 8b	0.018	0.028	0.046	0.056	0.049	0.06
fig. 9	-0.05	-0.02	-0.036	-0.014	-0.16 <sup>a)</sup>	-0.19 <sup>a)</sup>
fig. 10	0.025	0.044	0.07	0.088	0.08	0.098

<sup>a)</sup> Here we use  $M^2 = 5$  and  $M^2 = 2$ , since for this diagram  $s/M^2$  plays the same role as  $M^2$  in the other case.

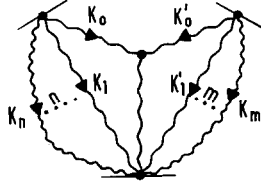


Fig. 7. Pomeron cuts which lead to the eikonal formula, eq. (17).

with respect to the pole contribution. The results are listed in table 1. Looking at the numbers and its variation over the range of energies, one notices that this kind of pomeron cut contribution is rather large at low energies and only slowly decreases as the energy goes up. This has already been found by the authors of ref. [6]. The reason why the two-pomeron cut in the triple-Regge region is much larger than the two-pomeron exchange in the two-body reaction  $pp \rightarrow pp$  can be traced back to simple combinatorics. In two-body scattering the two-pomeron exchange requires a  $1/2!$  because of statistics, whereas this factor is not present in the two-pomeron cut in the triple-Regge region. In the fourth row of table 1 we show the sum of all four contributions, the pole graph, fig. 6a and its complex conjugate, and fig. 6b. According to our rules, fig. 6a occurs with a negative sign, while fig. 6b is positive again. Because of the strong two-pomeron cut, the result is very small. It is, roughly, the square of [pole graph minus the graph of fig. 6a].

There are two conclusions to be drawn from this result. The first is that estimates of the size of cut corrections, based on the experience from two-body physics, cannot directly be applied to the triple-Regge region. Secondly, because of the strength of the two-pomeron cut correction, higher orders of pomeron exchanges need to be taken into account (fig. 7). This suggests to use the eikonal formula for the sum of  $n$ -pomeron exchanges, derived by several authors [4,6,11]. It is easy to obtain this expression with the reggeon calculus, and we derive it in our appendix:

$$\frac{1}{16\pi s^2} |\xi_{\alpha(q^2)}|^2 \int d^2 b_1 d^2 b_2 e^{iq(b_1 - b_2)} \times S(s, b_1) S(s, b_2) Y(s/M^2, M^2, b_1, b_2), \tag{17}$$

with

$$Y(s/M^2, M^2, b_1, b_2) = \frac{i}{(2\pi)^4} \int d^2 k_1 d^2 k_2 g \cdot g \cdot g \cdot r e^{-i(k_1 b_2 - k_2 b_2)} \times \left(\frac{s}{M^2}\right)^{\alpha(k_1^2) + \alpha(k_2^2)} (M^2)^{\alpha((k_1 + k_2))^2}, \tag{18}$$

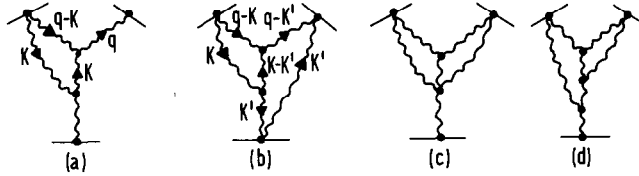


Fig. 8. Enhanced diagrams of eqs. (20) and (21).

$$S(s, \mathbf{b}) = \exp \left\{ -\frac{1}{(2\pi)^2} \int d^2 k e^{-i\mathbf{k} \cdot \mathbf{b}} g^2(k^2) s^{\alpha(k^2)-1} \right\}. \tag{19}$$

This eikonal formula holds for the “elastic” inclusive reaction  $a + b \rightarrow c + \text{anything}$  with  $c = a$ , where only pomerons are exchanged. It agrees with the expression of ref. [6]. For the case  $c \neq a$ , however, the basic exchange is that of a non-vacuum reggeon, and the eikonal approximation does not precisely specify how to approximate the vertex particle  $a - \text{particle } c - n \text{ pomerons-reggeon}$ . The basic assumption of the eikonal approximation means that, between the successive pomeron exchanges, only the elastic intermediate state should be included. But in our case this leaves it open whether to use  $(g_a)^n g_{aRc} / 2^{n/2}$  or  $g_{aRc} (g_c)^n / 2^{n/2}$  for the vertex (here  $g_a, g_c$  are the pomeron couplings to particle  $a$  and  $c$  resp., and  $g_{aRc}$  the reggeon particle coupling). Using the latter choice, one arrives at the result of ref. [4]. The expression of ref. [11] can hardly be justified from this point of view, since contributions appear to be overcounted.

In practice, one expands the exponentials of  $S(s, \mathbf{b})$  in (17). Table 1 then tells us that at low energies this expansion will converge rather slowly, whereas at higher energies the convergence will improve.

The next class of diagrams we wish to consider are graphs with one additional triple-pomeron coupling, in particular the enhanced diagrams. The first graph is that of fig. 8a. It is the (simply) enhanced version of fig. 6a\*.

As to the square of this graph, one has both fig. 8c and fig. 8d. The first one contains a four-pomeron coupling, the size of which we do not know. The other one is double enhanced and contains already three triple-pomeron couplings. In our present considerations we will omit both of them and rather include that of fig. 8b. It contains a pomeron cut contribution on both sides of the diagram and has one more triple-pomeron coupling than the diagrams considered previously. The expressions at  $q^2 = 0$  of figs. 8a and b have the form

$$F_{\text{pole}} \frac{g_0^2}{16\pi\alpha'} \frac{r_0}{g_0} \ln \frac{\ln s + (A + 2B)/2\alpha'}{\ln(s/M^2) + (A + 2B)/2\alpha'}, \tag{20}$$

\* Fig. 8a is obtained from fig. 6a by inserting a pomeron exchange into the pomeron-particle pomeron-particle amplitude at the bottom of fig. 6a. This makes the graph of fig. 8a more singular than fig. 6a and “enhances” the high-energy behavior of fig. 8a.

for fig. 8a, and for fig. 8b

$$\begin{aligned}
 F_{\text{pole}} & \left( \frac{g_0^2}{8\pi\alpha'} \right)^2 \frac{r_0}{g_0} \frac{1}{4 C_1^{1/2}} \ln(1 + C_2), \\
 C_1 & = \left( \frac{A+B}{\alpha'} + \ln s \right) \left( \frac{3A+2B}{2\alpha'} + \ln s + \ln(s/M^2) \right), \\
 C_2 & = 4C_1^{1/2} \ln M^2 \left[ 4 \left( \frac{A+B}{\alpha'} + \ln s \right) \left( \frac{A+2B}{2\alpha'} + \ln(s/M^2) \right) \right. \\
 & \quad \left. - \left( \frac{B}{\alpha'} \right)^2 + 2 \ln M^2 \left( \frac{2A+B}{2\alpha'} + \ln s \right) - 2C_1^{1/2} \ln M^2 \right]^{-1}. \tag{21}
 \end{aligned}$$

Let us first compare eq. (20) with (12). For large  $\ln s$ , eq. (12) behaves like  $F_{\text{pole}}/\ln s$ , whereas formula (20) goes with  $F_{\text{pole}} \ln \ln s$  (for fixed  $s/M^2$ ). This demonstrates the well-known fact that enhancement “enhances” the large- $s$  behavior by a factor  $\ln s \ln \ln s$ . For finite  $s$ , however, the enhancement effect is lowered by the small triple-pomeron coupling  $r$  as well as the log factor in (20). For small  $\ln s$  and  $\ln(s/M^2)$ , the argument of the log factor is close to one and leads to a rather small value of eq. (20). The same argument also applies to eqs. (13) and (21).

Numerical values for the factor multiplying  $F_{\text{pole}}$  in (20) and (21) are listed in table 1. Comparing the graphs of figs. 6a and 8a, we find that at low energies enhancement (i.e. the transition from non-enhanced graphs to enhanced ones) reduces the magnitude of a graph by a factor  $\frac{1}{10}$ . At highest ISR energies, however, the enhanced graphs reach already  $\frac{1}{2}$  of their non-enhanced counterparts. The same relation holds between enhanced and non-enhanced diagrams that have pomeron exchanges on both sides (figs. 6b and 8b). We also notice a variation with  $M^2$ . The enhanced graphs become most important for large values of  $M^2$ . Our main conclusion is that, for  $s \geq 1000 \text{ GeV}^2$ , enhanced graphs (i.e. those with one additional triple-pomeron coupling) start to become important. Depending on the desired accuracy of the analysis, it may even be necessary to include graphs with one more triple-pomeron coupling.

There are still two diagrams left that have two triple-pomeron couplings (figs. 9 and 10). The first one at  $q^2 = 0$  is obtained from eq. (20) by interchanging  $\ln(s/M^2)$

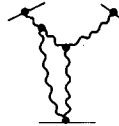


Fig. 9. The enhanced graph of eq. (22).

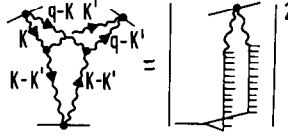


Fig. 10. The enhanced graph of eq. (23).

and  $\ln M^2$ :

$$F_{\text{pole}} \frac{g_0^2}{16\pi\alpha'} \frac{r_0}{g_0} \ln \frac{\ln s + (A + 2B)/2\alpha'}{\ln M^2 + (A + 2B)/2\alpha'} \quad (22)$$

For the other one we obtain

$$F_{\text{pole}} \left( \frac{g_0^2}{8\pi\alpha'} \right)^2 \frac{r_0}{4g_0 C_3} \ln(1 + C_4),$$

$$C_3 = \frac{A + B}{\alpha'} + \ln s,$$

$$C_4 = 4C_3 \ln M^2 \left[ 4C_3^2 - 2C_3 \ln M^2 - \left( \frac{A + B}{\alpha'} + \ln M^2 \right) \left( \frac{A + B}{\alpha'} + 2 \ln M^2 \right) \right]^{-1} \quad (23)$$

Again we find that at low energies they are about 10% of non-enhanced diagrams and go up to 50% at  $s = 3000 \text{ GeV}^2$ . The graph of fig. 9 also rather strongly depends on  $M^2$ . In contrast to that of fig. 8a, however, its size becomes larger for small  $M^2$ , i.e. large  $s/M^2$ . In fig. 8a, the enhancement affects the  $j$ -channel, and  $M^2$  being the energy variable conjugate to  $j$  must be as large as possible in order to stress the effect of enhancement. In fig. 9 it is the  $j_1$  channel in which enhancement takes place, and  $s/M^2$  now plays the same role as  $M^2$  before.

Finally, a word is in place about the  $q^2$  dependence of our diagrams. For the pole graph, the  $q^2$  dependence is shown in (11) and has, for small  $q^2$ , the form  $e^{-q^2\alpha_{\text{eff}}}$  with

$$\alpha_{\text{eff}} = A + B + 2\alpha' \ln(s/M^2). \quad (24)$$

Similarly, the  $q^2$  dependence of the other graphs can be described (at least for small  $q^2$ ) by an exponential  $e^{-q^2\alpha_{\text{eff}}}$ , where  $\alpha_{\text{eff}}$  depends on  $M^2$ ,  $s/M^2$  and varies rather strongly between the different graphs. In particular the diagrams of figs. 6b and 10 have a slope much smaller than the pole diagram. For larger values of  $q^2$ , therefore, these pomeron cut diagrams will be more important than the pole graph.

#### 4. Conclusions

To summarize the main results of our analysis, we order all our diagrams with respect to two properties. The first is the number of pomerons going down from the

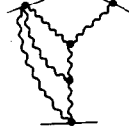


Fig. 11. A simply enhanced graph with an eikonal type cut correction.

top vertex to the bottom vertex (“eikonal pomeron”), the other the number of triple-pomeron couplings (“degree of enhancement”). At low energies, quite a large number of eikonal pomerons needs to be included, whereas enhancement is still irrelevant because of the smallness of the triple-pomeron coupling. When the energy goes up, the convergence of the eikonal expansion slowly improves, and, at the same time, enhanced diagrams start to be relevant. At very high energies, they eventually will be the only important contributions, and reggeon field theory is necessary to sum them up. Within this general picture, our analysis of the triple-Regge region determines where we stand with our present day energies ( $s \sim 3000 \text{ GeV}^2$ ). For an adequate description of the inclusive cross section, we still need several terms of the eikonal expansion. Because of the combinatorics the convergence is worse than in the  $2 \rightarrow 2$  case. On the other hand, eikonal graphs alone are not enough. Diagrams with at least one, if not two, additional triple-pomeron couplings must be included. Combining these two groups of diagrams, we conclude that also enhanced graphs with eikonal pomerons (fig. 11) have to be taken into account.

In so far the situation is quite similar to that found in the analysis of  $\sigma_{\text{tot}}$  of pp scattering [13]. What makes it different is the existence of an additional degree of freedom, the relative size of  $M^2$  and  $s/M^2$ . In particular the enhanced diagrams do depend on these variables, and depending on the kinematical region inside the triple-Regge region, different diagrams are the most important ones. On the whole one may say that cut corrections in the triple-Regge region have a much richer structure than in two-body reactions.

## Appendix

In this appendix we give a few details of our calculations. First we consider the graph of fig. 6a. The partial wave  $F(j_1, j_2, j, t)$  follows from the reggeon calculus and has the form

$$\begin{aligned}
 F(j_1, j_2, j, t) = & \frac{1}{(2\pi)^2} \int d^2 k N_2 \cdot N_2 \cdot r \cdot g \\
 & \times \frac{1}{j_1 - \alpha((q - k)^2) - \alpha(k^2) + 1} \frac{1}{j_2 - \alpha(q^2)} \frac{1}{j - 2\alpha(k^2) + 1} . \quad (\text{A.1})
 \end{aligned}$$

We insert this expression into the representation (4) and perform the  $j$ -integrations:

$$\begin{aligned} \frac{d^2\sigma}{dt dM^2} &= \frac{1}{16\pi M^2} \left(\frac{s}{M^2}\right)^{-\alpha' q^2} e^{-i\pi\alpha' q^2/2} \frac{1}{(2\pi)^2} \\ &\times \int d^2k N_2 \cdot N_2 \cdot r \cdot g e^{-\alpha'(\xi - i\pi/2)[(q-k)^2 + k^2]} e^{-2\alpha'\eta k^2}, \\ \xi &= \ln(s/M^2), \quad \eta = \ln M^2. \end{aligned} \tag{A.2}$$

Using the formulas (9), (10) and (14) for  $g$ ,  $r$ , and  $N_2$  respectively, (A.2) becomes

$$\begin{aligned} &\frac{1}{16\pi M^2} \left(\frac{s}{M^2}\right)^{-\alpha' q^2} e^{-i\pi\alpha' q^2/2} \frac{1}{2(2\pi)^2} \\ &\times \int d^2k g_0^5 r_0 \exp\left\{-\alpha' \left(\xi - \frac{1}{2}i\pi + \frac{A+B}{2\alpha'}\right) [(q-k)^2 + k^2]\right. \\ &\left. - 2\alpha' \left(\eta + \frac{A}{2\alpha'}\right) k^2\right\}. \end{aligned} \tag{A.3}$$

The  $k$ -integration can be transformed into a Gaussian integral and for  $q = 0$ , leads to eq. (12).

For the reggeon diagram of fig. 6b we proceed in the same way. For the partial wave we find

$$\begin{aligned} F(j_1, j_2, j, t) &= \frac{1}{(2\pi)^4} \int d^2k \int d^2k' N_2 \cdot N_2 \cdot N_3 \cdot r \\ &\times \frac{1}{j_1 - \alpha(k^2) - \alpha(q-k)^2 + 1} \frac{1}{j_2 - \alpha(k'^2) - \alpha((q-k)^2) + 1} \\ &\times \frac{1}{j - \alpha(k^2) - \alpha(k'^2) - \alpha((k-k')^2) + 2}. \end{aligned} \tag{A.4}$$

Doing the  $j$ -integrations we obtain

$$\begin{aligned} \frac{d^2\sigma}{dt dM^2} &= \frac{1}{16\pi M^2} g_0^7 r_0 \frac{1}{4(2\pi)^4} \int d^2k d^2k' \\ &\times \exp\left\{-\alpha'(\xi - \frac{1}{2}i\pi)[(q-k)^2 + k^2] - \alpha'(\xi + \frac{1}{2}i\pi)[(q-k')^2 + k'^2]\right. \\ &\left. - \alpha'\eta[k^2 + k'^2 + (k-k')^2] - \frac{1}{2}(A+B)[(q-k)^2 + (q-k')^2 + (k-k')^2]\right. \\ &\left. - A[k^2 + k'^2]\right\}. \end{aligned} \tag{A.5}$$

This leads to (13).

Next we derive the eikonal formula which represents the sum of graphs of fig. 7. For  $n$  pomerons on the left-hand side and  $m$  pomerons on the right-hand side the reggeon calculus leads to

$$\begin{aligned} \frac{d^2\sigma}{dt dM^2} &= \frac{1}{16\pi} |\xi_{\alpha(q^2)}|^2 \frac{(-1)^{n+m}}{n!m!} \int \prod_{i=0}^n \left[ \frac{d^2k_i}{(2\pi)^2} s^{\alpha(k_i^2)-1} \right] \\ &\times \prod_{j=0}^m \left[ \frac{d^2k'_j}{(2\pi)^2} s^{\alpha(k'_j{}^2)-1} \right] r N_{n+1} N_{m+1} N_{n+m+1} (M^2)^{\alpha((k_0+k'_0)^2)-\alpha(k_0^2)-\alpha(k'_0{}^2)} \\ &\times \delta^{(2)}\left(q - \sum_{i=0}^n k_i\right) \delta^{(2)}\left(q + \sum_{j=0}^m k'_j\right). \end{aligned} \quad (\text{A.6})$$

In the eikonal approximation only elastic intermediate states between pomeron exchanges are taken into account. Formally this is achieved by approximating the two-particle- $n$ -pomeron vertices by

$$N_n = g^n / 2^{(n-1)/2}. \quad (\text{A.7})$$

Using this approximation in (A.6) and expressing the two delta-functions in (A.6) by an impact parameter integral, one finds an analytic expression for the sum over  $n$  and  $m$ :

$$\begin{aligned} \frac{d^2\sigma}{dt dM^2} &= \frac{1}{16\pi} |\xi_{\alpha(q^2)}|^2 \int d^2b d^2b' e^{iq(b-b')} \\ &\times \sum_{n=0}^{\infty} \frac{(-1)^n}{n!} \left[ \int \frac{d^2k}{2(2\pi)^2} e^{-ikb} g^2(k^2) s^{\alpha(k^2)-1} \right]^n \\ &\times \sum_{m=0}^{\infty} \frac{(-1)^m}{m!} \left[ \int \frac{d^2k'}{2(2\pi)^2} e^{-ik'b'} g^2(k'^2) s^{\alpha(k'^2)-1} \right]^m \\ &\times \int \frac{d^2k_0 d^2k'_0}{(2\pi)^4} e^{-i(k_0b - k'_0b')} \left(\frac{s}{M^2}\right)^{\alpha(k_0^2) + \alpha(k'_0{}^2) - 2} \\ &\times (M^2)^{\alpha((k_0+k'_0)^2) - 2} \cdot r \cdot g \cdot g \cdot g. \end{aligned} \quad (\text{A.8})$$

This is just eq. (17).

Next we come to the enhanced graphs. Fig. 8a yields

$$\begin{aligned} F(j_1, j_2, j, t) &= \int \frac{d^2k}{(2\pi)^2} N_2 \cdot g \cdot g \cdot r \cdot r / \sqrt{2} \\ &\times \frac{1}{j_1 - \alpha((q-k)^2) - \alpha(k^2) + 1} \frac{1}{j_2 - \alpha(q^2)} \\ &\times \frac{1}{j - 2\alpha(k^2) + 1} \frac{1}{j - \alpha(0)}. \end{aligned} \quad (\text{A.9})$$

The last two denominators are combined:

$$\frac{1}{j - 2\alpha(k^2) + 1} \frac{1}{j - 1} = \int_0^1 dx \frac{1}{(j - 1 + 2x\alpha'k^2)^2} \quad . \quad (\text{A.10})$$

It is now easy to perform the  $j$ -integrations:

$$\begin{aligned} \frac{d^2\sigma}{dt dM^2} &= \frac{1}{16\pi M^2} g_0^4 r_0^2 \int_0^1 dx \ln M^2 \int \frac{d^2k}{2(2\pi)^2} \\ &\times \exp \left\{ -\alpha' \xi [(q - k)^2 + k^2] - 2\eta x \alpha' k^2 - \frac{1}{2}(A + B) [(q - k)^2 + k^2] - Bk^2 \right\} . \end{aligned} \quad (\text{A.11})$$

The  $k$ -integral is of Gaussian type, and the  $x$ -integral is done at the end. The result is (20).

The remaining graphs (fig. 8b and fig. 10) are evaluated in the same way, and we give only the expressions for the partial waves. For fig. 8b we find

$$\begin{aligned} F(j_1, j_2, j, t) &= \int \frac{d^2k d^2k'}{(2\pi)^4 \sqrt{2}} N_2 \cdot N_2 \cdot N_2 \cdot r \cdot r \frac{1}{j_1 - \alpha(k) - \alpha((q - k)^2) + 1} \\ &\times \frac{1}{j_2 - \alpha(k'^2) - \alpha((q - k')^2) + 1} \frac{1}{j - \alpha(k^2) - \alpha(k'^2) - \alpha((k - k')^2) + 2} \\ &\times \frac{1}{j - 2\alpha(k'^2) + 1} . \end{aligned} \quad (\text{A.12})$$

The expression for fig. 10 is

$$\begin{aligned} F(j_1, j_2, j, t) &= \frac{1}{2} \int \frac{d^2k d^2k'}{(2\pi)^4 \sqrt{2}} \frac{N_2 \cdot N_2 \cdot N_2 \cdot r \cdot r}{j_1 - \alpha(k^2) - \alpha((q - k)^2) + 1} \\ &\times \frac{1}{j_2 - \alpha(k'^2) - \alpha((q - k')^2) + 1} \frac{1}{j - 2\alpha((k - k')^2) + 1} \\ &\times \frac{1}{j - \alpha(k^2) - \alpha(k'^2) - \alpha((k - k')^2) + 2} . \end{aligned} \quad (\text{A.13})$$

## References

- [1] N.S. Craigie, G. Kramer and J. Körner, Nucl. Phys. B68 (1974) 509.
- [2] N.S. Craigie and G. Kramer, Nucl. Phys. B82 (1974) 69.
- [3] K. Ahmed, J.G. Körner, G. Kramer and N.S. Craigie, Nucl. Phys. B108 (1976) 275.
- [4] J. Pumplin, Phys. Rev. D13 (1976) 1249, 1261.
- [5] K.J.M. Moriarty, J.P. Rod, J.H. Tabor and A. Ungkitchanukit, Preprint Royal Holloway College (1976).
- [6] A. Capella, J. Kaplan and J. Tran Thanh Van, Nucl. Phys. B105 (1976) 333.

- [7] H.D.I. Abarbanel, J. Bartels, J.B. Bronzan and D. Sidhu, *Phys. Rev. D*12 (1975) 2798
- [8] J.L. Cardy, R.L. Sugar and A.R. White, *Phys. Letters* 55B (1975) 384.
- [9] H.D.I. Abarbanel, J. Bartels, J.B. Bronzan and D. Sidhu, *Phys. Rev. D*12 (1975) 2459
- [10] V.A. Abramovskij, V.N. Gribov and O.V. Kanchelli, *Proc. Batavia Conf.*, 1972.
- [11] N.S. Craigie, K.J.M. Moriarty and J.H. Tabor, CERN TH-2140.
- [12] R.L. Sugar and A.R. White, *Phys. Rev. D*10 (1974) 4063, 4074.
- [13] A. Capella and J. Kaplan, *Phys. Letters* 52B (1974) 448.